Visakhapatnam Chapter

Proceedings of Indian Geotechnical Conference 2020
December 17-19, 2020, Andhra University, Visakhapatnam

On Stress-Strain Function of Geomaterials Subjected to Blast-loads

Shashank Pathak[1] and G.V. Ramana[2]

[1.] Postdoctoral Researcher, Precision Mechatronics Laboratory, Université Libre de Bruxelles, 1050 Bruxelles, Brussels, Belgium; shashankpathaks@gmail.com

[2.] Professor, Department of Civil Engineering, Indian Institute of Technology Delhi, New Delhi-110016, India, gvramanaiitdelhi@gmail.com

Abstract. An appropriate stress-strain relationship of geomaterials subjected to blast loading is essential for the design of underground protective structures. Previous experimental and theoretical research efforts indicate that the constitutive behaviour of geomaterials under blast loading depends upon strain rate, stress level, and interaction among the three phases (solid, liquid, and gases). In current state-of-the-art, various advanced constitutive models are available to model the stress-strain behavior of geomaterials under blast-loads. However, considering the cost of computation associated with such models, a functional form is discussed to model the loading and unloading branches of stress-strain curve of geomaterials subjected to blast load based on three parameters: weight factor, initial modulus ratio, and strain recovery ratio. It is
observed that the new functional form reasonably captures the mean trend of the experimentally obtained or simulated stress-strain data. This paper further investigates the applicability of this functional form and provides a catalogue of the model parameters for direct use by practicing engineers. The dependence of function parameters on strain-rate, lateral confinement, degree of saturation, initial compaction, and locking-initiation stress is investigated and some simple rules are proposed for reasonable estimation of the three parameters. The proposed functional form would be quite useful in practical design problems specially where cost of computation associated with advanced constitutive models is too high. In addition to this, the proposed simple parametrization of complex nonlinear stress strain behaviour also provides an opportunity to investigate the effect of uncertainties in soil parameters in a computationally efficient manner.

Keywords: Blast load, Hyperbolic model, Constitutive model, SHPB, High strain rate, Functional-form.

1 Introduction

The uniaxial stress-strain behavior of geomaterials subjected to high strain-rate loading is of vital importance in the design of blast-resistant underground structures. Geomaterials subjected to blast-loads are generally exposed to high stresses and high strain-rates. High strain-rates significantly affect the geomaterial stiffness, strength, and other mechanical behaviours (Casagrande and Shannon 1948, Whitman 1970, Jackson

et al. 1980, Prapaharan et al. 1989, Yamamuro and Lade 1993, Bolton et al. 1994, Semblat et al. 1999, Omidvar et al. 2012). The duration of blast loading is very short which is not enough for water and entrapped gases to flow out. Therefore, undrained conditions exist under blast loading due to which the effective stress approach does not remain valid (*e.g.*, Wang and Lu 2003, Wang et al. 2004a, An et al. 2011).

Various experimental studies such as Bleich and Weidlinger (1963), Durbin (1964), Hampton and Wetzel (1966), Schindler (1968), Farr (1986, 1990), and Omidvar et al. (2012) have shown that the initial response of geomaterials subjected to high strain rate loading is mainly governed by the elastic deformations at the contact points of particles. With increasing load, the particles cannot rearrange into a denser configuration due to extremely short loading time and a significant portion of the applied energy is absorbed by the deformation of soil particles and volumetric compression which in turn causes stiffening (or strain-hardening) of the geomaterials. Durbin (1964) analyzed the wave propagation velocities in laterally confined sand columns and observed that initial stress waves propagate at faster velocities compared to the waves corresponding to higher stresses. However, beyond a certain stress level, wave propagation velocity increases with stress. This indicates that the configuration of the stress-strain curve of geomaterials subjected to blast loads should be reverse-S-shaped as shown in Fig. 1. This hypothesis was later on supported by another experimental study on Ottawa sand (Hampton and Wetzel 1966) in which the soil specimens were loaded by high-pressure waves and the resulting stress-strain curve showed an yielding nature below a certain threshold stress level and a stiffening behavior above that level.

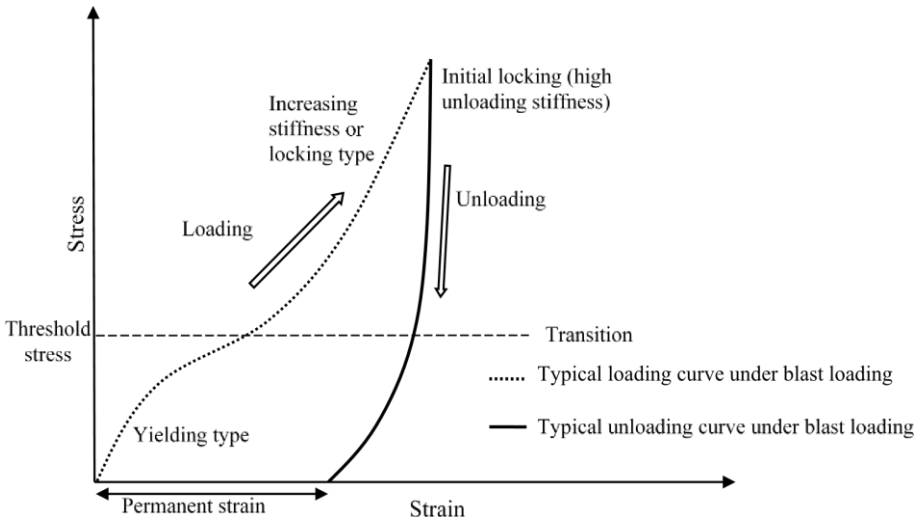

Fig. 1. Typical stress-strain diagram of geomaterials subjected to blast type loading (modified from Pathak and Ramana 2018a)

The above discussed experimental observations are also supported by geomechanics view-point (Henrych 1979, Wang and Lu 2003, Wang et al. 2004a) in which soil is treated as a three phase medium and the deformation of geomaterials is explained to occur through two processes: (i) the deformation of bonds between the solid particles at initial (low) stress levels and the failure of bond and particle displacement with increasing stress, and (ii) volumetric compression of the three soil phases at higher stresses. However, the relative contribution of the two deformation mechanisms depends upon: (a) the relative proportion of the solid, liquid and gaseous phases in the soil or degree of saturation, and (b) the magnitude of the applied stresses. Thus, the deformation behavior of a dry sand (low degree of saturation) and saturated clay (high degree of saturation) under blast-loading would be different and, similarly, the behavior of soils near the point of explosion (high stress zone) would be different compared to the soils at a farther distance from point of explosion (low stress zone).

On the other hand, a review of relevant studies (Salvadori et al. 1960, Rohani 1999) indicates that the unloading behavior is stiffer than the loading behavior at all stress levels except at low stresses where a sharp breaking tail occurs and, after complete unloading, permanent strains occur in the geomaterial (Fig. 1).

Several advanced constitutive models have been developed by various researchers to define the behaviour of geomaterials under blast load or high strain-rate loading. Though such models are quite insightful, those are computationally tedious and involve a number of parameters which need to be calibrated through various experimental studies. To reduce the computational efforts for routine applications, recently the authors (Pathak and Ramana 2018) proposed a simple functional form to capture the experimental or simulated stressstrain curves mathematically.

This paper investigates and explores the applicability of the Pathak-Ramana functional form in a great detail. A catalogue of the model parameters is developed, based on different strain-rates and degree of saturation, for direct use by practicing engineers. The dependence of model parameters on strain-rate, lateral confinement, degree of saturation, initial compaction, and locking-initiation stress is discussed and simple models are developed for estimation of model parameters based on locking-initiation stress. The practical applicability of the stress-strain function is also demonstrated through a case-study of an atmospheric nuclear test (Shot Priscilla) in which nuclear-air-blast-induced ground displacements are estimated.

2 A Brief Summary of Advanced Constitutive Models for Blast Loading

Constitutive modeling of soils under blast-loading has been an important area of research since the time of cold-war. Smith and Newmark (1958) developed a nonlinear spring-dashpot system to simulate the nonlinear constitutive behavior of soils subjected to nuclear-blastinduced overpressures. Since then various improved and advanced constitutive models have been developed to model the behavior of geomaterials under blast or high strain-rate loading

(Lu and Fall 2018). Some notable studies are Wang and Lu (2003), Wang et al. (2004a, b, 2008), Lewis (2004), Grujicic et al. (2006, 2008a, b), Tong and Tuan (2007), Feldgun et al. (2008a, b, 2011, 2013), Karinski et al. (2009a, b), An et al. (2011), and Higgins et al. (2013).
The development of such constitutive models usually involves equation of state (e.g., Lyakhov 1974, Wang and Lu 2003, Wang et al. 2004a, 2004b, 2008, 2011, Feldgun et al. 2008b, 2011), and a failure and strength model (*e.g.*, Simo et al. 1988, Lewis 2004, Wang et al. 2004a, Ghassemi et al. 2010, Feldgun et al. 2013, Xu and Zhang 2015, Lu and Fall 2017).

However, such advanced modeling techniques are computationally intensive and costly as multiple material models are required to be used along with various iterative computations. For example, the model of Tong and Tuan (2007) is a viscoplastic cap model of the Perzyna type with an associative viscous flow rule to represent the time-dependent behavior of soils. The model is based on 12 material parameters, namely, (1) a fluidity parameter in viscoplastic flow rule, (2) an exponent of viscous flow function, (3) a normalizing constant with the same unit as plastic yield function, (4, 5, 6, 7) four parameters in the cap surface, (8, 9, 10, 11) four material parameters in the failure surface, and (12) a tension cut-off parameter. In addition to this, bulk modulus and shear modulus are also required to determine the elastic part of the response. These parameters are determined from various tests such as uniaxial strain test, dynamic uniaxial strain tests with different strain rates, and triaxial compression tests at different confining pressures. Subsequently, these parameters are plugged into equations of (a) viscoplastic flow rule, (b) cap surface, (c) failure surface, and (d) tension cut-off surface and then the desired stress-strain curve is determined by solving these equations simultaneously, using various computational techniques such as fully implicit or explicit integration scheme, Newton–Raphson iteration process, etc. This long and tedious computational procedure makes these models unattractive to the practicing engineers and, therefore, the applicability of these models remain limited to either research studies or only highly specialized projects that involve the use of advanced computational tools. Even after using such advanced models there are serious limitations such as (i) a single model cannot replicate the behaviour of geomaterials at all the locations since the blast loading conditions (strain rate and magnitude of stress) are spatially variable, and (ii) inadequate experimental data is also a major limitation in the further verification of these advanced models for different soil types. In addition to this, the model parameters determined from limited experimental investigations are subjected to inherent variability of the naturally occurring and randomly arranged geomaterials in horizontal and vertical directions (Lumb 1974, Vanmarcke 1977, Phoon and Kulhawy 1999a, b, Elkateb et al. 2003).

3 Functional Forms for Stress-Strain Models

In view of the above, for routine engineering applications, experimental or simulated stress strain curves may be approximated by appropriate functional forms. Various useful functional forms of stress-strain behavior of geomaterials have been developed

in the past and are also being used in routine geotechnical engineering problems. For example, the hyperbolic approximation for idealizing the triaxial compression stress-strain curve was first developed by Kondner (1963) and later on used by many researchers due to its simplicity (*e.g.*, Duncan and Chang 1970, Mellah et al. 2000, Mei et al. 2017, Baek et al. 2017). Similarly, spline functions (Desai 1971, Cheek et al. 1971) have also been used to approximate the nonlinear stress-strain relationships of soils. Puzrin and Burland (1996) proposed a logarithmic function for the experimental stress-strain curves of soils and rocks.

However, the basic philosophy behind the development of the above stress-strain functions is different from the present case of blast-load. For computing nuclear-air-blast induced ground displacement, Nowatzki (1965) used the Ramberg-Osgood model (1943) arguing that it reasonably models the initial yielding portion of the experimentally determined stress-strain curve. Later, Rohani (1999) studied stress-strain relationships of soils under stress wave propagation and discussed about (i) piecewise-linear fit, (ii) nonlinear locking type model (Weidlinger and Matthews 1965), (iii) linear hysteretic model (Skalak and Weidlinger 1961), and (iv) nonlinear hysteretic model (Hendron 1963). However, none of the above mentioned stress-strain functions completely captures the experimental stress-strain behavior (Fig. 1) of geomaterials under blast-loads.

4 Proposed Functional Form

A preliminary investigation by the authors suggests that following functional form can be successfully used to define the uniaxial stress-strain curve of geomaterials subjected to blast loads (Pathak and Ramana 2018). The functional form is developed in terms of normalized stress ($y=\sigma/\sigma_p$) and normalized strain ($x=\varepsilon/\varepsilon_p$), where, σ is the stress, σ_p is the peak stress, ε is the strain and ε_p is the peak strain. A brief summary of the functional form is as follows:

4.1. Loading curve

The reverse-S-type loading curve (Eq. 1) is the weighted mean of an appropriate hyperbolic (Kondner 1963) and a non-linear hysteretic (Hendron 1963) type curve (Fig. 2).

$$y = \frac{wx}{wr_i + (1 - wr_i)x} + (1 - w)x^{1/r} \tag{1}$$

where, w, r_i, and r, are the three model parameters, namely, weight factor, initial modulus ratio, and strain recovery ratio. The weight factor reflects the relative contribution of yielding and strain-hardening components in the overall stress-strain curve. The yielding component (first term in Eq. 1) is represented by a hyperbolic curve, whereas, the strain-hardening is represented by a nonlinear hysteretic curve

(second term in Eq. 1). The parameter *w* is qualitatively related with the threshold stress at which the governing deformation mechanism changes (Fig. 1).

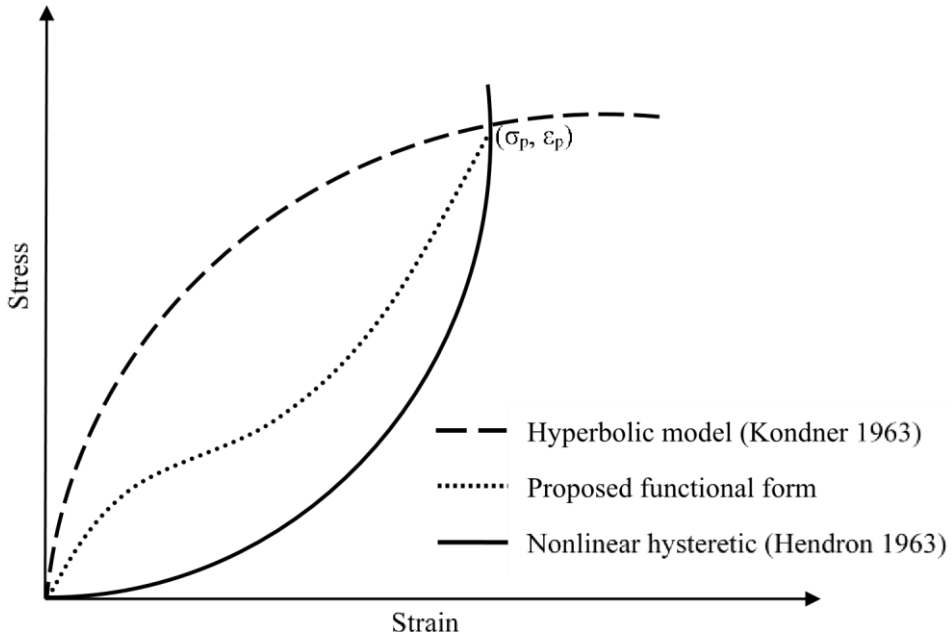

Fig. 2. Functional forms of loading stress-strain curves of geomaterials

The parameter *w* can take any value in the range 0 to 1. However, an approximate value of *w* can be chosen based on a qualitative comparison of the experimental curve with the five typical cases as shown in Fig. 3. It is observed that for lower values of parameter *w*, there is an early initiation of stiffening or strain-hardening type behavior or sharp increase in the tangential modulus. This is also termed as locking behaviour of geomaterials under high strain rate loading (Veyera 1994). This happens due to the fact that when *w* reaches closer to zero, the weightage of locking behavior increases and at w=0, Eq. 1 simplifies to only strain hardening component where parameter r_i becomes redundant and parameter *r* decides the rate of strain hardening. On the other hand, as *w* increases and becomes equal to 1, then only yielding behaviour governs and the third parameter *r* becomes redundant in the loading curve (Eq. 1). Thus, the value of parameter *w* also indicates the initiation of the locking behavior.

The second parameter r_i referred to as initial modulus ratio is the ratio of the secant modulus (at peak stress) to the tangent modulus (at initial stress) and reflects the average change in stiffness of the geomaterial with increasing stress. Practically, this parameter can take any real positive value. The loading constraint (or secant) modulus and initial tangent modulus are two important geotechnical parameters required for

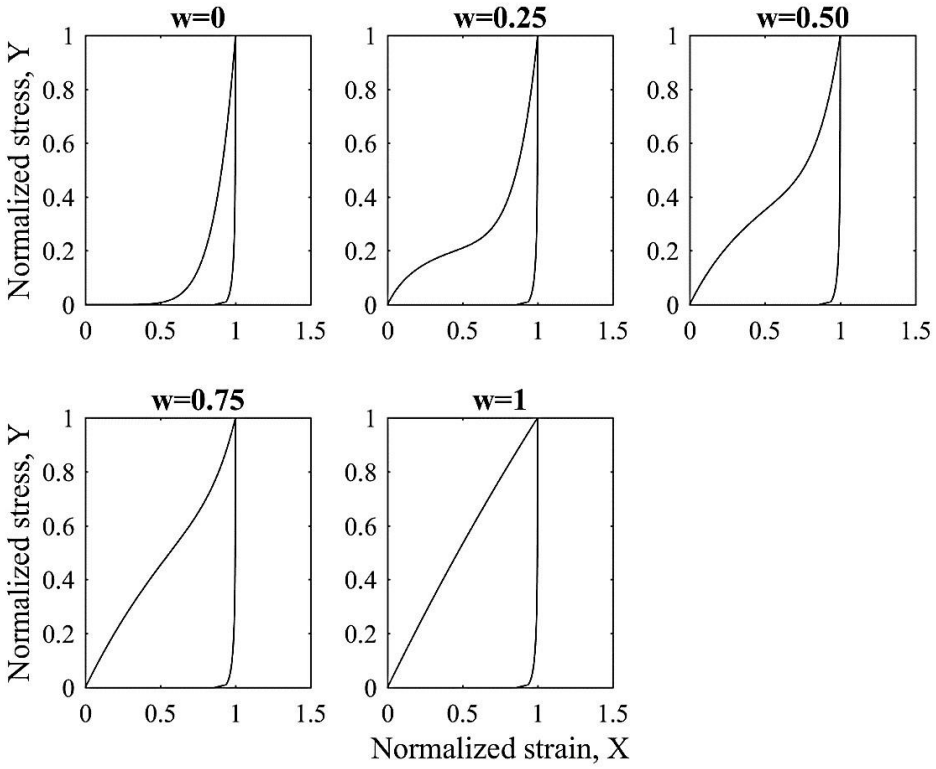

Fig.3. Normalized stress-strain curves for different values of parameter *w* (modified from Pathak and Ramana 2018a)

estimation of r_i. Various experimental techniques can be used for determination of constrained modulus such as observed ground motions, seismic velocity test, dynamic one-dimensional compression test, triaxial test, resonant column test, and plate bearing test. Discussion on advantages and limitations of these techniques can be found in Wilson and Sibley (1962), Whitman (1970), and Frye and Lipner (1983). However, Whitman (1970) highlighted that the value of constrained modulus based on any single technique does not provide the representative value and a combined interpretation of the results obtained from all of the above mentioned tests is required to obtain the representative value. A detailed discussion on selection of constrained modulus at various depths below ground surface can be found in Wilson and Sibley (1962). However, the initial tangent modulus may be obtained directly from the information on density profile and P-wave propagation of geomaterials considering the fact that the modulus at initial stresses is proportional to the square of the seismic wave velocity (Kramer 1996).

The third parameter *r* is the ratio of the secant modulus (loading constrained modulus) to the unloading secant modulus (unloading constrained modulus) which is also equal to the ratio of recovered strain upon unloading to the peak strain upon

loading. Therefore, this parameter is also referred to as strain recovery ratio. However, in case of loading curve this parameter mainly determines the rate of strain-hardening or locking behavior. The parameter *r* can assume values in the range of 0 to 1. The value zero represents pure locking behavior with no strain-recovery upon unloading, whereas, the value one represents the pure elastic behavior with 100% strain-recovery upon unloading. Thus, a smaller (or higher) value of parameter *r* corresponds to higher (or smaller) rate of strain-hardening in loading curve. The typical values of the strain recovery ratio for various types of test is mentioned in Wilson and Sibley (1962) as ~0.30 for confined compression tests with slow loading, ~0.60 for confined compression tests with fast loading, and ~1.0 for vibration tests and seismic velocity tests.

4.2 Unloading curve

The unloading curve is represented (Eq. 2) through the weighted mean of a nonlinear hysteretic curve (Hendron 1963) and a locking curve (Salvadori et al. 1960) in such a way that the locking effect reduces with decreasing stress (Fig. 4).

$$x = 1 - \frac{r^2(1-y)(1-y^r)}{(r+y-2ry)} \tag{2}$$

where, *r* is the strain recovery ratio (*i.e.*, same as the third parameter *r* in case of loading curve Eq. 1). If *r* =0 (no strain recovery) then Eq. 2 reduces to *x*=1, *i.e.*, locking behaviour upon unloading. Similarly, if *r*=1 (100% strain recovery) then Eq. 2 reduces to *x*=*y*, *i.e.*, linear elastic behaviour.

In view of the above, the three parameters can be calibrated based on an appropriate uniaxial testing of the geomaterial sample. Then the proposed functional form can be fitted to the recorded stress-strain data. The three parameters can be obtained using a hit and trial procedure. The initial guess for starting the hit and trial procedure can be made using the following guidelines:

a) Use Fig. 3 for selecting initial value of parameter *w*.

b) Evaluate the ratio of loading secant modulus to the unloading secant modulus or the value of strain recovery ratio for selecting initial value of parameter *r*.

c) The initial value of parameter r_i can be taken as the ratio of secant modulus to initial tangent modulus

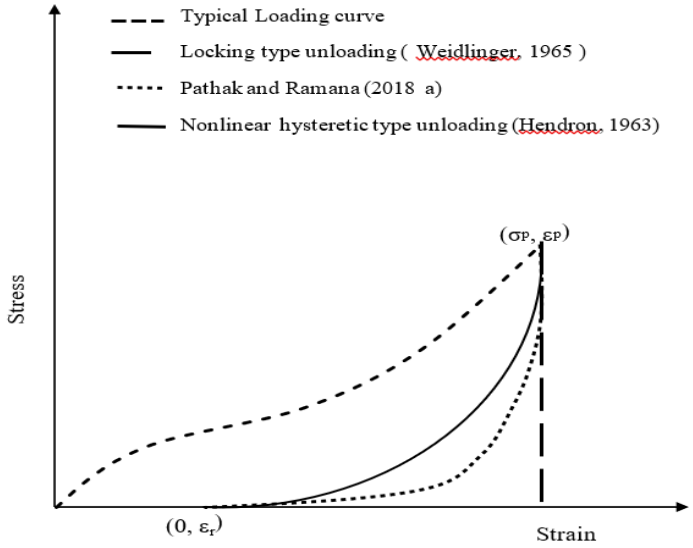

Fig.4. Functional form of unloading stress-strain curves of geomaterials.

5 The Function Parameters

The parameters of the Pathak-Ramana stress-strain function can be estimated by fitting the experimental stress-strain data. Since the function parameters have well defined physical meaning and can be estimated through simple procedures as discussed above, therefore, any complicated nonlinear regression analysis or optimization procedure are not required. However, in a few cases some fine-tuning of model parameters may be required to improve
the quality of the fit.

In this paper, a wide variety of experimental data on the uniaxial stress-strain response of various geomaterials is compiled and digitized from published literature (Table 1). The
Pathak-Ramana stress-strain function is fitted to these experimental data and the corresponding parameters are obtained as listed in Table 1. Some of the fitted stress-strain curves are shown in Figs. 5-9 and it is observed that the proposed function reasonably captures the experimental data. The experimental and simulated data (Table 1) considered in this study consists of (i) partial saturated calcite sand subjected to high strain rate and static test, (ii) SHPB test of dry fine-silica sand under varying degree of confinement, (iii) SHPB test of fine-quartz sand with varying degree of saturation, (iv) simulated stress-strain curve of dry sand subjected to shock wave based on Hugoniot data, (v) SHPB test on Eglin, Tyndall, and Ottawa sands with varying degree of

saturation and strain-rates, (vi) SHPB test of quartz sand and glass beads with varying degree of saturation and strain-rates, (vii) static and SHPB tests on volcanic ashes with varying degrees of confinement and initial compaction, (viii) simulated SHPB tests on Ottawa and Fontainebleau sand at different strain-rates, (ix) dynamic 1-D compression test on Till, (x) SHPB tests on a dry Ottawa sand at different strain rates, (xi) uniaxial compression tests on partially saturated calcite and flume sand and siltyclay at different stress-rates, (xii) uniaxial static compression of quartz, Cambria, and gypsum sands with different initial compaction upto a stress level around 800 MPa, (xiii) uniaxial dynamic compression test on Playa silt, (xiv) static uniaxial compression of Minnesota sand, (xv) uniaxial compression of McCormick Ranch sand and sandy-clay, (xvi) uniaxial compression of a fine-grained soil, (xvii) uniaxial loading and unloading of alluvium and a sandy clay, (xviii) uniaxial compression of sandy-silt caused by an air-blast, (xix) SHPB test on dry silica sand and a polycarbonate material at different strain-rates, (xx) SHPB test on alluvium and clayey-sand, and (xxi) uniaxial stress-strain curve of soils at a nuclear test site at Nevada. Various relevant details on these experimental records can be found in the footnotes of Table 1.

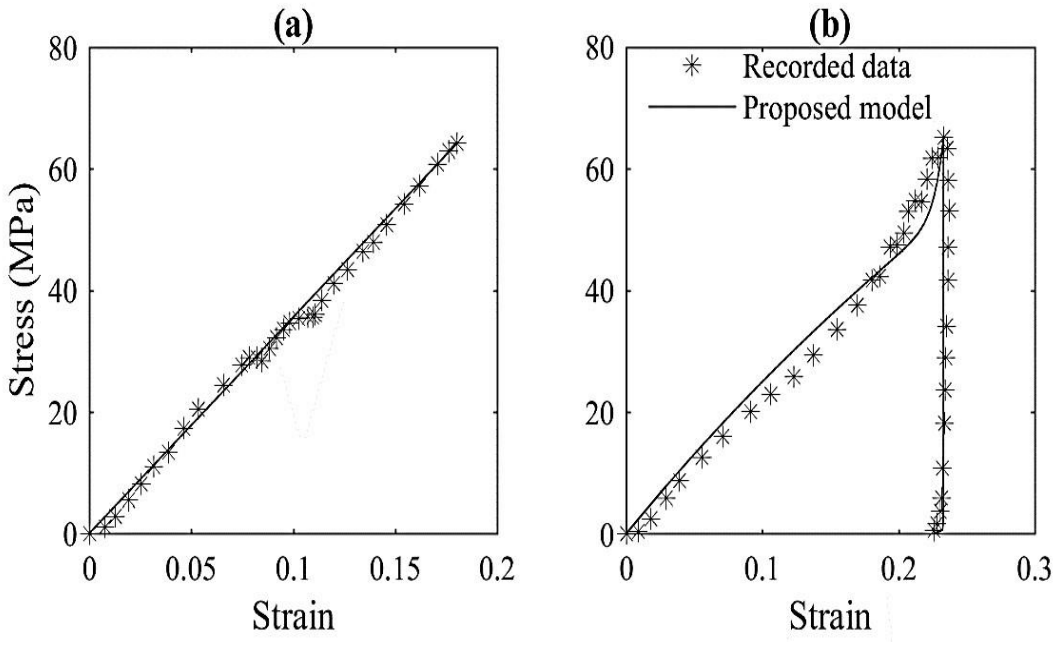

Fig.5. Pathak-Ramana stress-strain function fitted to experimental uniaxial stress-strain data of Calcite sand (Akers 1986) under (a) high strainrate and (b) static test

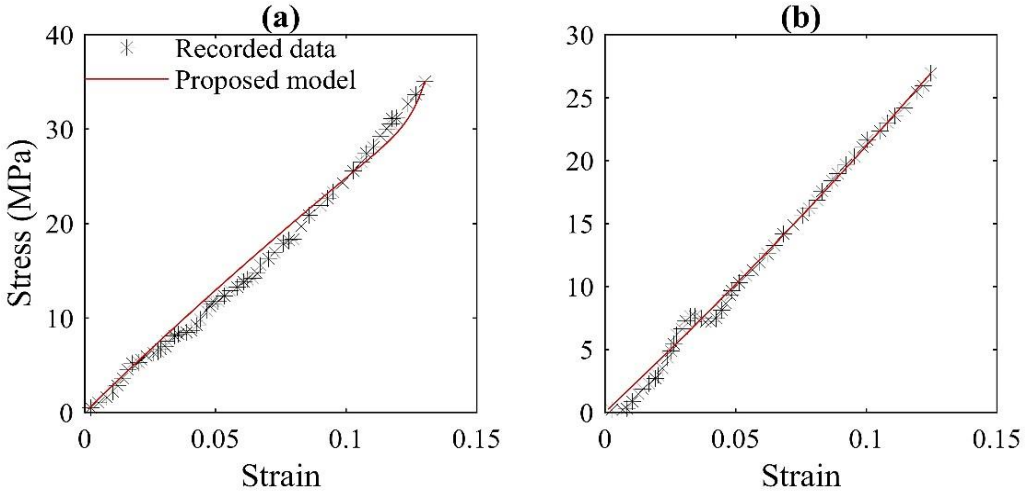

Fig.6. Pathak-Ramana stress-strain function fitted to SHPB test data of Fine silica sand (Song et al. 2009) with (a) steel tube confinement, and (b) Polycarbonate Tube confinement

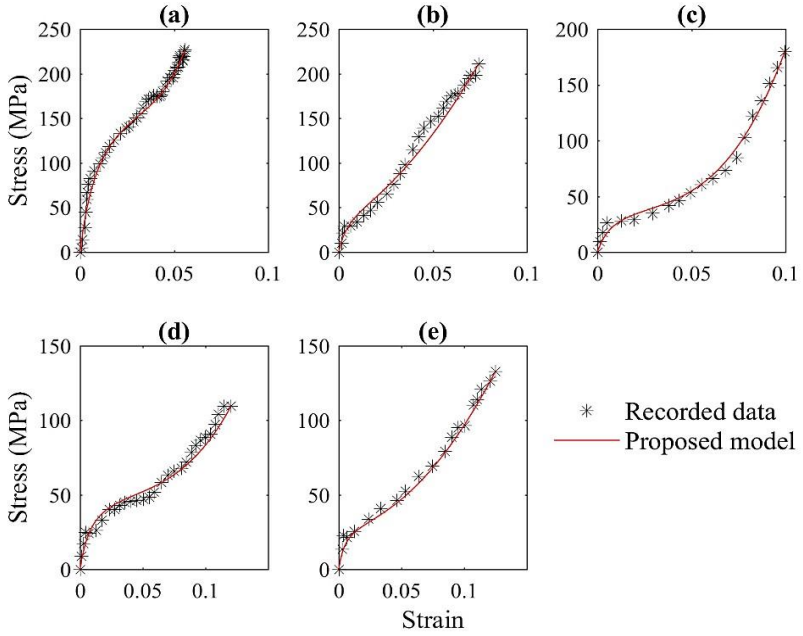

Fig. 7. Pathak-Ramana stress-strain function fitted to SHPB test (at 1000/sec strain rate) data of (a) 100% saturated, (b) 80% saturated, (c) 60% saturated, (d) 20% saturated, and (e) dry Eglin sand adopted from Veyera (1994)

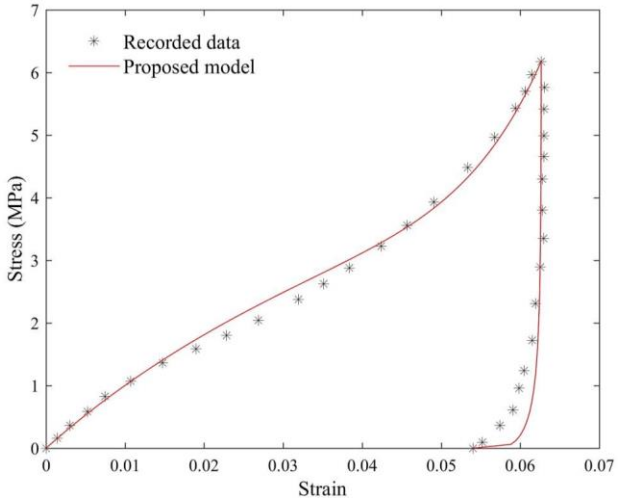

Fig. 8. Pathak-Ramana stress-strain function fitted to dynamic 1-D test data of partially saturated Till adopted from Jackson (1968).

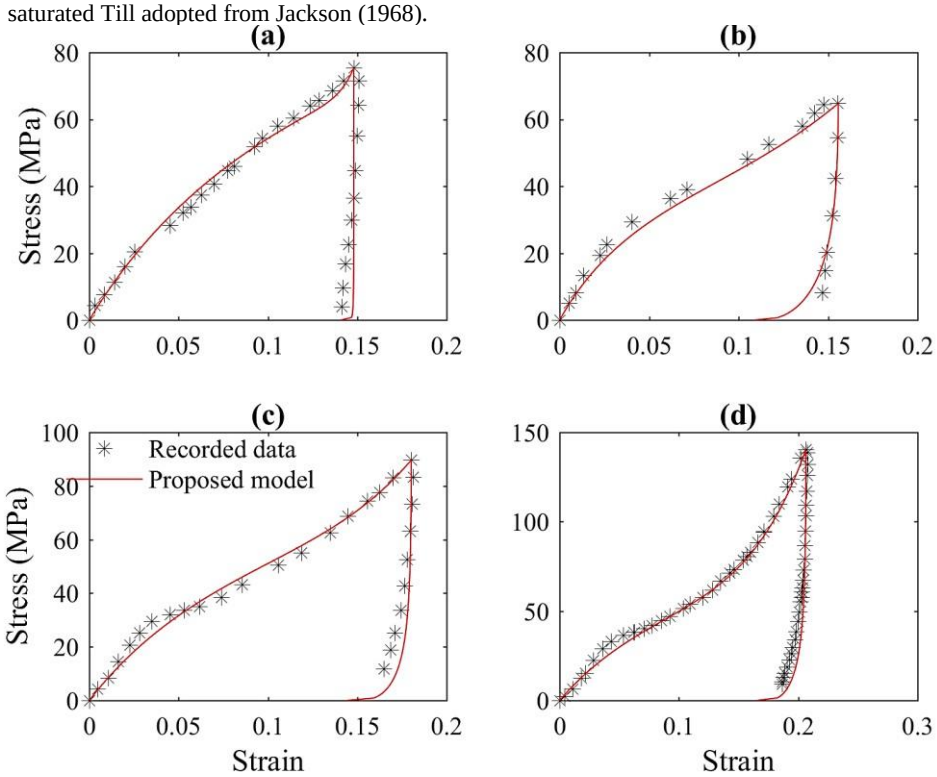

Fig. 9. Pathak-Ramana stress-strain function fitted to SHPB test data of dry Ottawa sand with strain rate of (a) 970/sec, (b) 1100/sec, (c) 1700/sec, and (d) 2100/sec adopted from Xia et al. (2015).

In Table 1, the experimental data is categorized based on the (i) type of geomaterials, (ii) observed locking behavior, (iii) approximate locking initiation stress, (iv) applied peak stress, (v) strain-rate, (vi) testing technique used to obtain the experimental data, and (vii) degree of saturation. It is observed that the Pathak-Ramana model fits reasonably well to the experimental and simulated stress-strain data of a variety of soil types subjected to a variety of loading and boundary conditions. The wide variety of data also provides an opportunity to analyze the effect of various loading and boundary conditions on the three function parameters. In addition to this, the prepared catalogue of the function parameters can also be used directly by the designers. It may be noted that in Section 4.1, it is clearly explained that the parameter w varies between 0 and 1, parameter r varies between 0 and 1 and parameter r_i can assume any positive value, theoretically. It is interesting to note that for compiled case studies in Table 1, the parameter w varies from 0 to 1, parameter r varies from 0.02 to 0.99, and parameter r_i varies from 0.11 to 45.53. A detailed discussion on the function parameters is as follows:

5.1 Effect of strain rate

To explicitly explore the effect of strain rate on model parameters, those case-studies are selected in Table 1 in which other essential parameters such as the type of soil and degree of saturation remain constant. It is observed that parameter w increases (or yielding behavior becomes significant) with increasing strain rate beyond a certain degree of saturation, whereas, below a certain degree of saturation, the parameter w decreases (or locking behavior becomes significant) with increasing strain rate. Parameter r_i increases with strain rate either at very high saturation or for dry sands, however, at partial saturated conditions, it decreases with increasing strain rate. Parameter r generally increases (or elastic recovery increases) with increasing strain rate under partially saturated conditions. Thus, it is clear that three function parameters depend significantly on applied strain-rate. For example, the parameters would vary with the distance from explosion-center for a given type of geomaterial.
However, a detailed systematic study is warranted for arriving at more specific conclusions.

5.2 Effect of saturation

Water is highly incompressible and air present in the voids does not offer significant resistance to the high strain-rate loading due to which the stress-strain response of geomaterials is significantly affected by the degree of saturation. For example: fully saturated sands exhibit a stiffer response compared to dry or unsaturated sand under high strain-rate loading (Whitman 1970). To exhibit a locking type stress-strain response, it is a prerequisite that the loading produces sufficient strain for particle rearrangement (Omidvar et al. 2012).

To examine the effect of degree of saturation, the relevant case-studies are selected from Table 1 for carrying out a parametric study. Variation of the three parameters with degree of saturation is plotted in Fig. 10 for different types of sand

subjected to different strain-rates. It is noted that parameter *w* is, generally, small (0.39 on average) at 20%-80% degree of saturation and locking behavior is observed. This indicates that sands at intermediate degree of saturation may exhibit locking behavior (e.g., Omidvar et al. 2012). In case of initial modulus ratio, a significant variation is seen for quartz sands with varying degree of saturation compared to other types of sands. For quartz sand, all the three parameters are observed to be decreasing with increasing degree of saturation. It is observed that type of sand and strain rate plays an important role in defining the dependence of function parameters on degree of saturation.

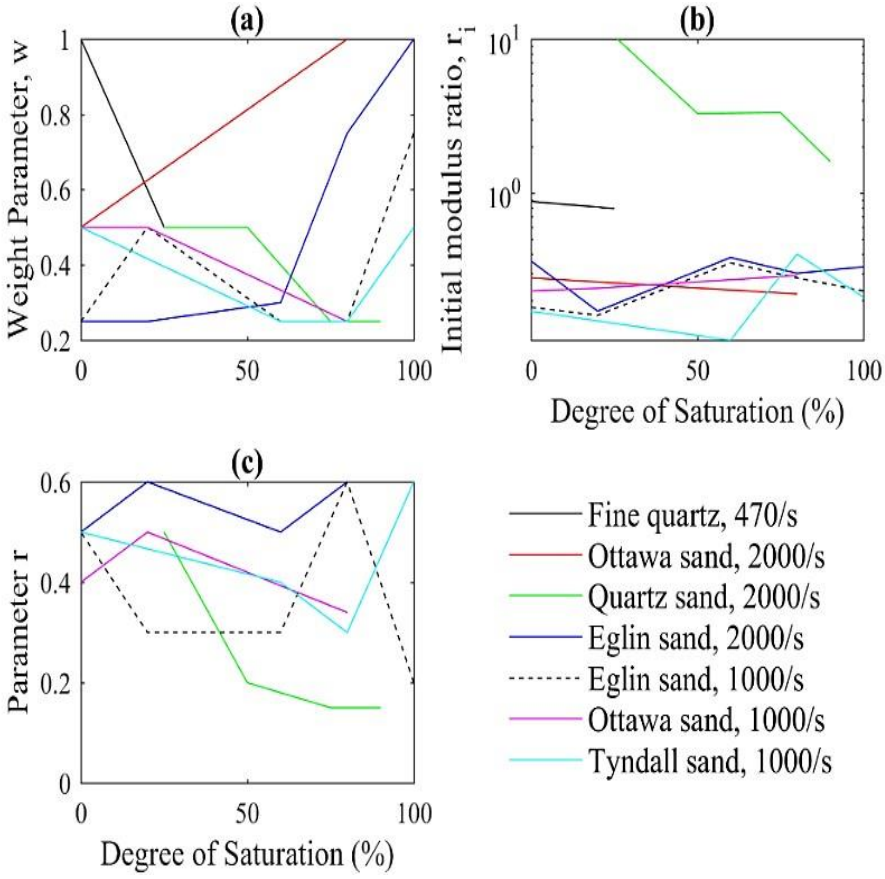

Fig.10. Variation of parameter (a) *w*, (b) r_i (semi-log), and (c) *r* with degree of saturation for different sands and strain rates

5.3 Effect of lateral confinement

The confinement of the geomaterial is an important boundary condition and significantly affects the stress-strain response. Apart from the physical confinement, the lateral inertial effects would also add to the confinement in case of high strain rate loading. In case of ideal rigid confinement like steel tube, the load path would be a uniaxial strain and locking type behavior would be observed, whereas, for softer confinement such as Polycarbonate tube or latex confinement, higher radial strains would occur and the condition would deviate from the uniaxial strain. In addition to this, the sample may fail in shear if adequately soft confinement is used (*e.g.*, Goh et al. 1998). From the appropriate case-studies in Table 1, it is found that for dry silica sand, the three parameters are nearly the same for rigid and loose confinements. However, for Etnean volcanic ash, all the three parameters reduce with reducing confinement. This indicates that there is no specific trend, possibly due to the effect of inertia that has been ignored in these limited case-studies. In addition to this, the different soil types may have different effects under different degrees of confinement. This analysis clearly indicates that the three function parameters would also vary with depth (due to increasing confinement) when the function would be used in practical problems.

5.4. Effect of initial compaction

The parameter r_i represents the average change in stiffness of the geomaterial with increasing stress. Stiffness of a loose sample may undergo a large change compared to a densely compacted sample with increasing stress. In other words, a loose sample is expected to have significantly lower initial stiffness compared to a dense sample due to which the loose sample exhibits significantly higher r_i values compared to dense sample. For example, in case of volcanic sand (Table 1), it is observed that for loose samples r_i values are 1.9 to 13 times more than the dense samples. Similarly, loose samples of Quartz, Cambria, and Gypsum sand exhibit 1.5, 2.5, and 3.8 times higher r_i values compared to a dense sample, respectively (see Table 1).

Loose samples are generally expected to have high rate of strain hardening compared to dense samples, therefore, loading curves of loose samples are expected to be associated with a smaller value of parameter r (Eq. 1). Thus, it is observed that parameter r decreases by a factor varying between 0.5 and 0.8 (at different strain rates) for volcanic sand with decreasing initial compaction. Similarly, in case of Quartz, Cambria, and Gypsum sands, parameter r decreases by a factor of 0.7, 0.7, and 0.3, respectively, with decreasing compaction. It can also be noted, that a loose sample would provide less strain recovery upon unloading compared to a dense sample which would also cause a smaller value of parameter r in case of loose samples.

In case of parameter w, no change is observed with varying level of initial compaction except in a single case of Gypsum sand for which weight factor increases by a factor of 2.8 with decreasing compaction.

5.5 Relation of the parameter 'w' with the locking-initiation stress

It is discussed previously in Section 4.1 that the parameter *w* can be related with locking behavior. In the present section, this hypothesis is investigated further. Based on all the case studies discussed in Table 1, the variation of parameter *w* is plotted against the ratio of locking-up initiation stress to peak stress (denoted as γ) as shown in Fig. 11. It is observed that *w* lies in the intervals [0-0.1], [0.25-0.30], [0.50-0.65] and [0.75-0.90] when γ falls in the intervals [0-0.12], [0.07-0.37], [0.19-0.67], and [0.56-0.93], respectively. Thus, parameter *w* is directly proportional to γ with a correlation coefficient of 0.86. In cases, where no locking up type behavior is observed (see Table 1), the average value of *w* is obtained as 0.83 with a coefficient of variation of 29%. If locking-up initiates at a very early stage of loading (*i.e.*, γ <<1), then a higher weight to strain hardening component is required in the loading curve

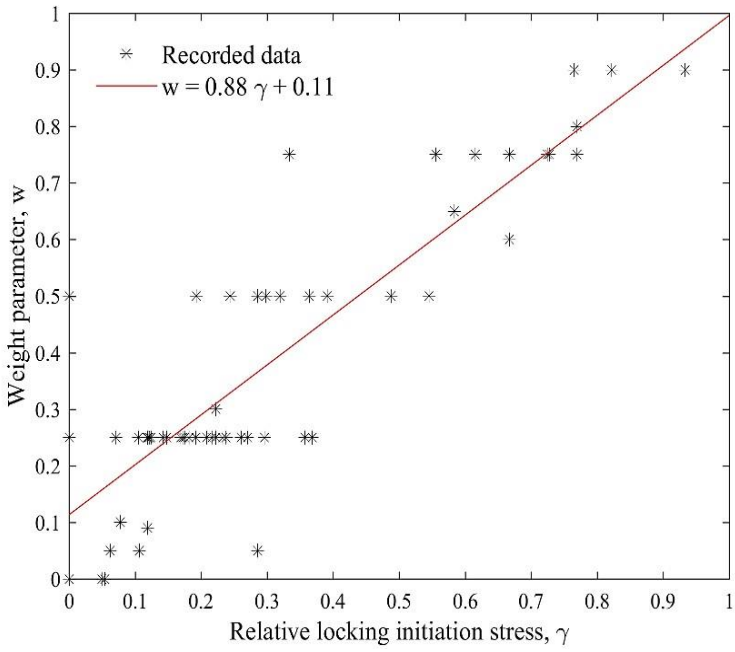

Fig. 11. Dependence of weight parameter on locking initiation stress (relative to peak stress)

(Eq. 1), and, therefore, in such cases, *w* approaches to zero. If locking-up type behavior initiates near peak stress (*i.e.*, $\gamma \sim 1$) or does not occur at all, then, in those cases the weight of the strain hardening component reduces significantly in loading curve, and *w* approaches to 1. For example, the average value of *w* (=0.83) corresponding to 'no locking-up type' cases falls in the last set of *w* [0.75-0.90] in Fig. 11. Thus, for the purpose of design, the parameter *w* can be scaled as given by Eq. 3 when locking-up type behavior is expected to initiate and when locking-up type behavior is not expected to initiate then the average value of *w* can be taken as 0.83.

$$w = 0.88\gamma + 0.11 \tag{3}$$

5.6 Relation of the parameter 'r_i' with the locking-initiation stress

The early initiation of locking-up (*i.e.*, γ <<1) may cause a significant increase in stiffness of the soil that may further increase the secant loading modulus of the soil due to which the value of the parameter r_i increases. Thus, for a smaller value of γ, a larger value of r_i is expected and, therefore, a decaying power-law type relation (Eq. 4) is observed between the parameter r_i and γ as shown in Fig. 12 with a correlation coefficient of 0.61.

$$r_i = 0.28(\gamma - 0.1)^{-0.87} \tag{4}$$

It is to be noted that Eq. 4 is valid only for the cases in which initiation of locking-up behavior has been observed in the experimental stress-strain data. For cases where locking-up has not been observed at all, the average value of parameter r_i is obtained to be 0.75 with a very high coefficient of variation of 55%. Such a high variation indicates that soil type plays an important role in deciding the parameter r_i in cases where locking-up does not initiate within applied strain levels.

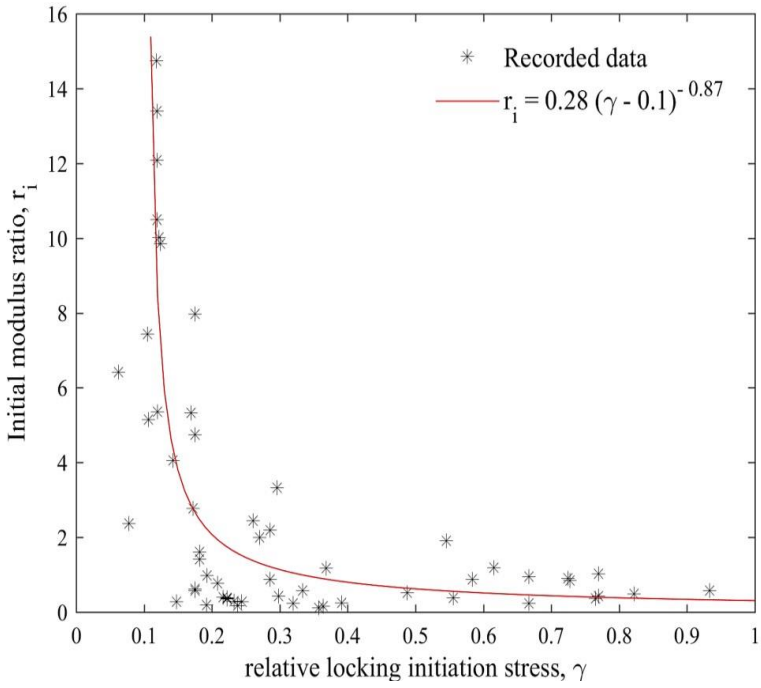

Fig. 12. Dependence of initial modulus ratio on locking initiation stress (relative to peak stress)

5.7 Relation of the parameter 'r' with the locking-initiation stress

The parameter *r* is directly related with the residual strain (in unloading curve) and the rate of strain hardening (in loading curve) but it is not directly related to the initiation of the locking up behavior. However, for the design purpose, five cases can be considered: (case-1) locking up type behavior is observed in unloading curves, (case-2) locking-up initiates in loading curve, (case-3) locking-up is not observed in unloading curve, (case-4) locking-up does not initiate in loading curve and (case-5) locking-up does not initiate in loading curve but upon unloading locking-up is observed. The average value of *r* for each case, respectively, is found to be 0.14, 0.25, 0.47, 0.37, and 0.08 with a coefficient of variation of 58%, 60%, 29%, 80%, and 74%, respectively. It is evident from the above analysis that the value of *r* becomes very small (such as 0.14 and 0.08) when locking-up is observed in unloading curves. The most precise average *r* (=0.47) is obtained (with 29% coefficient of variation) for cases where locking-up is not observed in unloading curve, and this is the highest average among all the 5 cases. Thus, it can be inferred that (on an average) $r \geq 0.47$ indicates that no locking-up is expected to occur in unloading curve. In such cases, locking-up is not expected to be observed in loading curves also because when locking-up does not initiate in the loading curve, then average *r* is 0.37 (<0.47). In addition to this, the rate of strain hardening (proportional to 1/*r*, See Eq. 1) reduces with increasing *r*. Therefore, it is expected that with higher values of *r* (probably more than 0.47 on an average) the locking-up will not be observed in both the loading and unloading curves. More confidence on these values can be gained by evaluating the model parameters for more number of case studies.

6 Function Parameters for Advanced Constitutive Models

The parameters of the stress-strain function can also be determined for simulated stress-strain behaviour using advanced constitutive models. For illustration, two examples are considered. In the first example, the function is fitted to the simulated stress-strain curve of sand subjected to shock wave based on typical Hugoniot data of sand (Omidvar et al. 2012) as shown in Fig. 13. In the second example, the function is fitted to the simulated SHPB stress strain data using the Higgins (2011) model for Ottawa sand as shown in Fig. 14. The constitutive model of Higgins (2011) is based on the concepts of (i) the bounding surface plasticity theory, (ii) Perzyna's viscoplasticity theory and (iii) the critical state soil mechanics and requires calibration of 21 constitutive parameters through triaxial compression tests, triaxial extension tests, Bender element tests, torsional hollow cylinder tests, and SHPB tests. It is observed from both the examples that the Pathak-Ramana function fits the simulated data reasonably well.

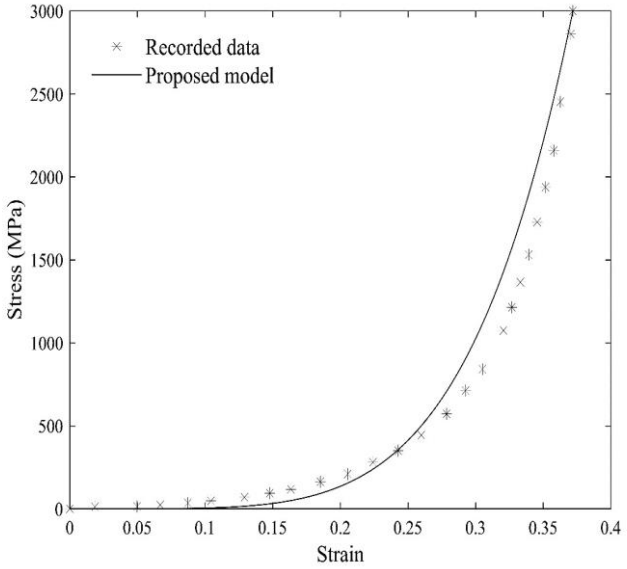

Fig.13. Pathak-Ramana stress-strain function fitted to simulated stress-strain curve based on typical Hugoniot data of sand (Omidvar et al. 2012)

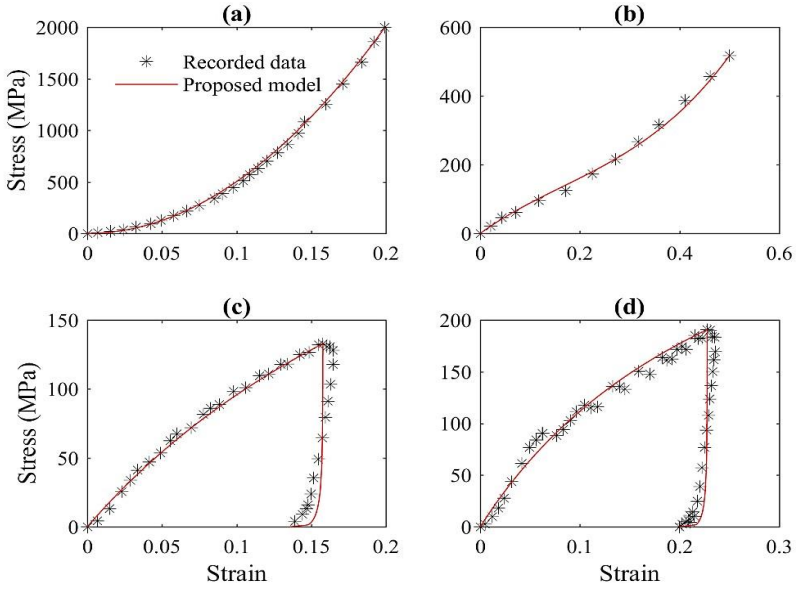

Fig.14. Pathak-Ramana stress-strain function fitted to simulated SHPB test data of Ottawa sand: with viscosity coefficient assumed as (a) 50,000 kPa-sec and (b) 0.5 kPa-sec (at fixed strain rate of 1000/sec) and strain rate taken as (c) 1000/sec and (d) 2000/sec (at fixed viscosity coefficient of 50 kPa-sec). All the simulated data is adopted from Higgins (2011).

It is worth noting that a separate study can also be carried out to investigate the relationship between various constitutive parameters of the advanced model and the three parameters of the Pathak-Ramana stress-strain function. For example: Higgins (2011) simulated the SHPB data on Ottawa sand for two extreme values (very high and very low) of viscosity coefficient (η_v). Therefore, it provided an opportunity to see the effect of viscosity coefficient on parameter *w*. It is intuitive that a very high η_v would significantly increase the resistance to plastic flow of the soil and strain hardening or locking type behavior would govern, whereas, a very low η_v would provide very less resistance to plastic flow upon yielding. Therefore, it can be seen from Table 1 that η_v= 50,000 kPa-sec corresponds to *w*=0, *i.e.*, strain hardening type behavior and η_v = 0.5 kPa-sec corresponds to a larger value of *w* (= 0.5) which indicates a significant contribution of yielding type behavior.

Table 1. A summary of experimental uniaxial stress-strain data and corresponding parameters of the proposed stress-strain function

Material	r_i	*r*	*w*	Lock-up observed (Y/N)	Approx. lock-up initiation stress (MPa)	Peak stress (MPa)	Strain rate/ rise-time/ duration	Test/ Technique/ Model	Saturation
Akers (1986)									
calcite sand[1]	1	--	1	N	--	65	3.62/ sec	High Strain Rate compression[2]	PS[3]
calcite sand[1]	1.02	0.03	0.8	Y(L)[#] Y(U)**	50	65	static	static compression	PS[3]
Song et al. (2009)									
Fine silica sand	1	0.04	0.9	N	--	35	upto1450/sec	SHPB test (steel tube confinement)	Dry
Fine silica sand	1.11	--	1	N	--	27	upto1450/sec	SHPB test (Polycarbonate Tube confinement)	Dry
Martin et al. (2009)									
fine quartz sand[1]	0.88	--	1	N	--	16	470/sec	SHPB test	Dry
fine quartz sand[1]	0.79	0.4	0.5	N	--	12	470/sec	SHPB test	25%

Omidvar et al. (2012)									
Sand[4]	--	0.2	0	Y	0	3000	Shock wave	Computed stress-strain curve using Hugoniot data	Dry
Veyera (1994)									
Eglin Sand[5]	0.23	0.2	0.75	Y	150	225	1000/sec	SHPB test[6]	100%
Eglin Sand[5]	0.28	0.6	0.25	Y	31	210	1000/sec	SHPB test[6]	80%
Eglin Sand[5]	0.35	0.3	0.25	Y	40	180	1000/sec	SHPB test[6]	60%
Eglin Sand[5]	0.16	0.3	0.5	Y	40	110	1000/sec	SHPB test[6]	20%
Eglin Sand[5]	0.18	0.5	0.25	Y	25	130	1000/sec	SHPB test[6]	Dry
Eglin Sand[5]	0.33	--	1	N	--	205	2000/sec	SHPB test[6]	100%
Eglin Sand[5]	0.30	0.6	0.75	N	--	230	2000/sec	SHPB test[6]	80%
Eglin Sand[5]	0.38	0.5	0.3	Y	50	225	2000/sec	SHPB test[6]	60%
Eglin Sand[5]	0.17	0.6	0.25	Y	50	210	2000/sec	SHPB test[6]	20%
Eglin Sand[5]	0.36	0.5	0.25	Y	50	225	2000/sec	SHPB test[6]	Dry
Tyndall Sand[7]	0.21	0.6	0.5	N	--	220	1000/sec	SHPB test[6]	100%
Tyndall Sand[7]	0.40	0.3	0.25	Y	40	185	1000/sec	SHPB test[6]	80%
Tyndall Sand[7]	0.11	0.4	0.25	Y	50	140	1000/sec	SHPB test[6]	60%
Tyndall Sand[7]	0.17	0.5	0.5	N	--	85	1000/sec	SHPB test[6]	Dry
Ottawa 20-30 Sand[8]	0.29	0.34	0.25	Y	50	215	1000/sec	SHPB test[6]	80%
Ottawa 20-30 Sand[8]	0.24	0.5	0.5	Y	45	115	1000/sec	SHPB test[6]	20%
Ottawa 20-30 Sand[8]	0.23	0.4	0.5	Y	40	125	1000/sec	SHPB test[6]	Dry
Ottawa 20-30 Sand[8]	0.22	--	1	N	--	220	2000/sec	SHPB test[6]	80%
Ottawa 20-30 Sand[8]	0.28	0.3	0.5	Y	50	205	2000/sec	SHPB test[6]	Dry
Water	1.13	--	1	N	--	230	1000/sec	SHPB test[6]	--
Wang et al. (2017)									
Soda-lime glass beads[9]	6.92	0.7	0.25	Y	0	105	1000-1300/sec	SHPB test	Dry

quartz sand[10]	1.41	0.4	0.25	Y	20	110	1500-1700/sec	SHPB test	Dry
quartz sand[10]	10.46	0.5	0.5	Y	0	130	1900-2100/sec	SHPB test	25%
quartz sand[10]	3.29	0.2	0.5	Y	0	140	1900-2100/sec	SHPB test	50%
quartz sand[10]	3.33	0.15	0.25	Y	40	135	1900-2100/sec	SHPB test	75%
quartz sand[10]	1.6	0.15	0.25	Y	20	110	1900-2100/sec	SHPB test	>90%
Pellegrino et al. (2016)									
Etnean volcanic ashes[11]	0.62	0.30	0.25	Y	10	57	~0.0005/sec	UTM on dense sample	--
Etnean volcanic ashes[11]	4.74	0.15	0.25	Y	10	57	~0.0005/sec	UTM on loose sample	--
Etnean volcanic ashes[11]	5.14	0.10	0.05	Y	5	47	~0.0005/sec	UTM with deformable confinement	--
Etnean volcanic ashes[11]	7.97	0.20	0.25	Y	10	57	~0.0005/sec	UTM with rigid confinement	--
Etnean volcanic ashes[11]	0.57	0.30	0.25	Y	10	57	~0.0005/sec	UTM with dense samples enclosed in rigid confinements	--
Etnean volcanic ashes[11]	7.43	0.17	0.25	Y	6	57	~0.0005/sec	UTM with loose assemblies restrained in rigid confinements	--
Etnean volcanic ashes[11]	6.41	0.08	0.05	Y	3	48	~0.0005/sec	UTM with loose samples enclosed in latex confinements	--
Etnean volcanic ashes[11]	2.77	0.25	0.25	Y	20	116	~1500/sec	SHPB test on dense samples	--

								enclosed in rigid confinements	
Etnean volcanic ashes[11]	5.33	0.20	0.25	Y	20	118	~1500/sec	SHPB test on loose assemblies restrained in rigid confinements	--
Etnean volcanic ashes[11]	2.37	0.20	0.1	Y	9	116	~1500/sec	SHPB test on loose samples enclosed in latex confinements	--
Higgins (2011)									
Ottawa sand	--	0.5	0	Y	100	1996	1000/sec	Simulated SHPB test with Viscosity coefficient 50000 kPa-sec	--
Ottawa sand	0.98	0.3	0.5	Y	100	518	1000/sec	Simulated SHPB test with Viscosity coefficient 0.5 kPa-sec	--
Ottawa sand	0.67	0.14	1	N (L)* Y(U)**	--	133	1000/sec	Simulated SHPB test	--
Ottawa sand	0.55	0.12	1	N (L) Y(U)	--	190	2000/sec	Simulated SHPB test	--
Fontainebleau sand12	0.54	0.35	1	N(L) N(U)	--	43	Simulated striker bar velocity of 6.8m/s	Simulated SHPB test	--
Fontainebleau sand[12]	0.49	0.11	0.9	Y(L) Y(U)	60	73	Simulated striker bar velocity of 11.6 m/s	Simulated SHPB test	--
Fontainebleau sand[12]	0.43	0.30	0.5	Y(L) Y(U)	40	134	Simulated striker bar velocity of 19.8m/s	Simulated SHPB test	--

Jackson (1968)									
Till[13]	0.88	0.14	0.65	Y(L) Y(U)	3.5	6	Dynamic test	Dynamic 1-D compression	78.3%
Xia et al. (2015)									
Ottawa sand[15]	0.58	0.05	0.9	Y(L) Y(U)	70	75	970/sec	SHPB test	Dry
Ottawa sand[14]	0.43	0.3	0.75	Y(L) Y(U)	50	65	1100/sec	SHPB test	Dry
Ottawa sand[14]	0.58	0.2	0.75	Y(L) Y(U)	30	90	1700/sec	SHPB test	Dry
Ottawa sand[14]	0.87	0.2	0.5	Y(L) Y(U)	40	140	2100/sec	SHPB test	Dry
Farr (1990)									
Calcite sand[16]	0.96	0.02	1	N (L) Y(U)	--	30	0.2 MPa/sec	Uniaxial compression	PS[3]
Calcite sand[16]	1.19	0.1	0.75	Y(L) Y(U)	40	65	2.9 MPa/sec	Uniaxial compression	PS[3]
Calcite sand[16]	0.9	0.2	0.75	Y(L) Y(U)	50	69	556 MPa/sec	Uniaxial compression	PS[3]
Flume Sand[17]	0.85	0.18	0.75	Y(L) Y(U)	40	55	0.4 MPa/sec	Uniaxial compression	PS[3]
Flume Sand[17]	0.51	0.25	0.5	Y(L) Y(U)	40	82	5750 MPa/sec	Uniaxial compression	PS[3]
silty clay[18]	1.9	0.3	0.5	Y(L) Y(U)	36	66	663 MPa/sec	Uniaxial compression	PS[3]
Yamamuro et al. (1996)									
Quartz Sand[19]	9.85	0.15	0.25	Y(L) Y(U)	100	807	Static tests	1-D Compression on dense sample	--
Quartz Sand[19]	10.01	0.1	0.25	Y(L) Y(U)	100	818	Static tests	1-D Compression on	--

								medium sample	
Quartz Sand[19]	14.74	0.1	0.25	Y(L) Y(U)	100	843	Static tests	1-D Compression on loose sample	--
Cambria Sand[20]	5.35	0.1	0.25	Y(L) Y(U)	100	835	Static tests	1-D Compression on dense sample	--
Cambria Sand[20]	10.5	0.09	0.25	Y(L) Y(U)	100	842	Static tests	1-D Compression on medium sample	--
Cambria Sand[20]	13.39	0.07	0.25	Y(L) Y(U)	100	840	Static tests	1-D Compression on loose sample	--
Gypsum Sand[21]	12.08	0.09	0.09	Y(L) Y(U)	100	839	Static tests	1-D Compression on dense sample	--
Gypsum Sand[21]	45.53	0.03	0.25	Y(L) Y(U)	60	842	Static tests	1-D Compression on loose sample	--
Hendron and Davisson (1964)									
Playa Silt[22]	0.77	0.2	0.25	Y	5	24	Dynamic test	1-D Compression	--
Hendron (1963)									
Minnesota sand[23]	0.38	0.19	0.75	Y(L) Y(U)	40	72	Static	Static loading	--
Jackson and Windham (1968)									
McCormick Ranch sand[24]	0.95	0.16	0.6	Y(L) Y(U)	4	6	--	Uniaxial strain	--
sandy clay[25]	--	0.45	0	Y(L) N(U)	0	4	--	Uniaxial strain	PS^3

Hendron et al. (1969)									
fine-Grained soil	2.00	0.17	0.25	Y(L) Y(U)	10	37	--	Uniaxial strain	PS3
Isenberg (1972)									
Alluvium[26]	--	0.2	0	Y(L)	0.0007	0.013	--	Loading	57%
Alluvium[26]	--	0.45	--	N(U)	--	0.013	--	Unloading	57%
Sandy clay[27]	4.05	0.25	0.25	Y(L)	2	14	--	Loading	--
Sandy clay[27]	--	0.65	--	N(U)	--	14	--	Unloading	--
McCormick et al. (1968)									
Sandy silt[28]	2.19	0.30	0.05	Y(L) N(U)	2	7	--	uniaxial strain due to air-blast	90%
Kabir et al. (2010)									
Silica sand[29]	1.04	0.04	1	N (L) Y(U)	--	33	470/sec	SHPB	Dry
Silica sand[30]	1.84	0.99	0.25	N	--	42	520/sec	SHPB	Dry
Silica sand[29]	0.71	0.35	0.5	N	--	65	900/sec	SHPB	Dry
Silica sand[29]	2.44	0.25	0.25	Y	50	192	1450/sec	SHPB	Dry
Polycarbonate[31]	0.36	0.2	0.9	Y	150	196	230-1660/sec	SHPB	Dry
Felice et al. (1991)									
Alluvium[32]	0.96	--	1	N	--	10	--	SHPB	initial moisture content 3%
Clayey sand[33]	1.17	0.2	0.25	Y	35	95	--	SHPB	initial moisture content 13.3%
Hadala (1973)									
Nevada Test Site[34]	0.55	0.6	0.75	N(L) N(U)	--	2	--	Uniaxial stress strain curve	--

1. Poorly graded,
2. Gas driven piston
3. Partially saturated
4. Density in front of the shock wave= 1.6 g/cm^3, speed of sound in geomaterial = 0.45 km/s, slope of the shock velocity vs. particle velocity curve =1.62
5. Sp. Gr. = 2.65, Dry density = 1450-1670 kg/m^3, Void ratio = 0.59-0.817.
6. Cannon pressure ~ 690 kPa, Square wave input stress ~ 225 MPa, Rise time to peak stress ~ 50 μs and a 257 μs pulse width.
7. Sp. Gr. = 2.65, Dry density = 1450-1630 kg/m^3, Void ratio = 0.621-0.817
8. Sp. Gr. = 2.65, Dry density = 1560-1720 kg/m^3, Void ratio = 0.545-0.705
9. Oven dried at 105°C Sp. Gr. = 2.50, Void ratio= 0.68
10. Poorly graded, sourced from Stockton Beach, Australia, Sp. Gr. = 2.65, Void ratio=0.68
11. Collected from the South-East flank of the volcano during the paroxysm of the 28th of December 2014, Mineral constituents: cristobalite and anorthite
12. Initial void ratio of 0.667
13. Undisturbed sample of Till, void ratio 0.382, Dry density = 1932 kg/m^3
14. Fine grained Ottawa sand, Grain density= 2.64 g/cc, Bulk Density= 1.6 g/cc, Void Ratio= 0.651
15. Coarse grained Ottawa sand, Grain density= 2.65 g/cc, Bulk Density= 1.66 g/cc
16. Sourced from Enewetak Beach Sand
17. Sp. Gr. = 2.64, Dry density=1.62 g/cc, water content =5.5%, Constituents=quartz with minor traces of potassium, feldspars, sillimanite, mica, smectite, clay-mica, kaolinite
18. Vicksburg Loess, Sp. Gr.= 2.71, Water content=11.5%, Dry density=1.63 g/cc, Constituents= quartz with minor traces of smectite, chlorite, vermiculite, clay-mica, kaolinite, palygorskite, plagioglase, potassium feldspars, and dolomite.
19. Mohs' hardness= 7, Grain size= 0.6-1.7 mm void ratio=0.66-1.07
20. Grain size=0.83-2 mm, Void ratio=0.49-0.78
21. Mohs' hardness= 2, Grain size= 0.075-1.18 mm, void ratio=0.7-0.97
22. Taken from the Nevada Test Site at Frenchman's Flat, Nevada
23. Initially loose sand Void ratio=0.619, Relative density =25%
24. A fine sand containing some silt and clay particles
25. from HEST Test V, Dakota
26. Layer 3 (1.2-2.7 m depth) of event middle gust-I (alluvium) initial void volume 33%
27. Layer 5 of middle gust site, porosity = 0.7%, (4.6-7.0 m), Density of middle Gust-sandy clay=2.08-2.16 gm/cc
28. Event 1A, operation distant Plain, layer III, wet sand, silt, depth 6-10.4m
29. Silica based fine grain, klin dried and poorly graded Sand, Density= 1.50 g/cc
30. Density=1.60 g/cc
31. PC material (polycarbonate), The 3.05-mm-thick circular PC tube was cut and separated into six equal parts as individual specimens in order to achieve consistency with the PC tube material used in the sand confinement experiments.
32. Initial density 1.77 g/cc from Yuma, Arizona

33. (initial density 2.12 g/cc) from McCormick Ranch Test Site at Kirtland AFB, New Mexico
34. Layer 1 at the Nevada Test Site, Density=1506 kg/m^3, P-wave velocity =335m/s, Depth=0-8.5 m

* No locking-up observed in loading curve
** Locking-up observed in unloading curve
# Locking-up observed in loading curve

7 Conclusions

In this paper, a detailed discussion and analysis is carried out related to the parameters of a newly proposed Pathak-Ramana stress-strain function for geomaterials subjected to high strain-loadings such as blast load. The stress-strain function is based on three parameters, namely: weight factor (w), strain recovery ratio (r), and initial modulus ratio (r_i). An exhaustive data set of experimental stress-strain curves of different types of geomaterials (sands, silts, and clays) with different types of conditions (dry, saturated, partially saturated, confined, and unconfined) subjected to various loads (dynamic loads, blast loads, impact loads, and static loads) is used to prepare a catalogue of the three model parameters. It is observed that the new functional form reasonably captures the mean trend of the stress-strain data corresponding to not only blast loads and high strain rates but also to static and dynamic loads. Based on the prepared catalogue of model parameters, following key conclusions are arrived at:

1. It is observed that the parameter w varies from 0 to 1, parameter r varies from 0.02 to 0.99, and parameter r_i varies from 0.11 to 45.53 for various case-studies considered in this paper.
2. The three function parameters are observed to be depending significantly on applied strain rate and, therefore, it indicates that the parameters would vary with the distance from explosion-center for a given type of geomaterial. However, a detailed systematic study is warranted for arriving at more specific conclusions.
3. It is also observed that soil type and applied strain-rate plays an important role in defining the dependence of function parameters on degree of saturation.
4. The study indicates that function parameters are also dependent upon the degree of confinement. This has an important implication that the three function parameters would also vary with depth (due to increasing confinement) when the function would be used in practical problems.
5. Since a loose sample is expected to have significantly lower initial stiffness compared to a dense sample, the loose samples are observed to be exhibiting significantly higher r_i values compared to dense samples. On the other hand, loose samples are generally expected to have high rate of strain hardening compared to dense samples, therefore, loading curves of loose samples are observed to be associated with a smaller value of parameter r compared to dense samples. However, in case of parameter w no specific conclusions could be obtained.
6. It is observed that w is directly proportional to the ratio of locking initiation stress to peak stress and a simple equation is proposed to estimate the weight factor.

However, in cases, where locking is not observed, the average value of weight factor is obtained as 0.83 with a coefficient of variation of 29%.

7. The early initiation of locking behaviour causes a significant increase in stiffness of the soil, and hence, increases the value of initial modulus ratio. Therefore, a decaying power-law type relation is proposed between initial modulus ratio and the ratio of locking initiation stress to peak stress. However, in cases, where locking is not observed, the average value of initial modulus ratio is obtained to be 0.75 with a coefficient of variation of 55%. Such a high variation indicates that soil type plays an important role in deciding the initial modulus ratio.
8. Generally, small value of parameter *r* (~0.1) correspond to the locking behaviour in unloading curves and large value (~0.5 or more) indicates that no locking is expected to occur in unloading as well loading curves.

The proposed functional form may prove to be quite useful in practical design problems specially where cost of computation associated with advanced constitutive models is too high. In addition to this, it may be noted that a simple parametrization of complex nonlinear stress-strain behaviour provides an opportunity to investigate the effect of uncertainties in soil parameters in a computationally efficient manner.

References

1. Akers, S. A. (1986). Uniaxial strain response of Enewetak Beach sand. Technical Report SL86-45. Vicksburg, MS: U.S. Army Engineer Waterways Experiment Station.
2. An, J., Tuan, C. Y., Cheeseman, B. A., and Gazonas, G. A. (2011). Simulation of soil behavior under blast loading. International Journal of Geomechanics, 11(4), 323-334.
3. Baek, S. H., Kim, J., Lee, S. H., and Chung, C. K. (2017). Development of the Cyclic py Curve for a Single Pile in Sandy Soil. Marine Georesources & Geotechnology.
4. Bleich, H. H., and Weidlinger, P. (1963). Stresses Waves in Granular Material. Weidlinger Associates New York.
5. Bolton, J. M., Durnford, D. S., and Charlie, W. A. (1994). One-dimensional shock and quasistatic liquefaction of silt and sand. Journal of geotechnical engineering, 120(10), 1874-1889.
6. Casagrande, A. and Shannon, W. L. (1948). Strength of soils under dynamic loads. Proc. Am. Soc. Civ. Eng. 74(4): 591–608.
7. Cheek Jr, J. B., Radhakrishnan, N., and Tracy, F. T. (1971). Application of Spline Interpolation Methods to Engineering Problems (No. WES-MP-8-71-2). Army Engineer Waterways Experiment Station Vicksburg Miss.
8. Desai, C. S. (1971). Nonlinear analyses using spline functions. Journal of the Soil Mechanics and Foundations Division, 97(10), 1461-1480.
9. Duncan, J. M., and Chang, C. Y. (1970). Nonlinear analysis of stress and strain in soils. Journal of the Soil Mechanics and Foundations Division,96(5), 1629–1653.
10. Durbin, W. L. (1964). Study of the Dynamic Stress-Strain and Wave-Propagation Characteristics of Soils; Report 2, Correlation of Stress-Strain and Wave-Propagation Parameters in Shock-Loading Dry Sands (No. 637-15). United Research Services Corp Burlingame CA.

11. Elkateb, T., Chalaturnyk, R., and Robertson, P. K. (2003). An overview of soil heterogeneity: quantification and implications on geotechnical field problems. Canadian Geotechnical Journal, 40(1), 1-15.
12. Farr, J. V. (1986). Loading rate effects on the one-dimensional compressibility of four partially saturated soils (No. WES/TR/SL-86-46). Army Engineer Waterways Experiment Station Vicksburg MS Structures Lab.
13. Farr, J. V. (1990). One-dimensional loading-rate effects. Journal of Geotechnical Engineering, 116(1), 119-135.
14. Feldgun VR, Karinski YS, and Yankelevsky DZ (2011). Blast pressure distribution on a buried obstacle in a porous wet soil. Int J Prot Struct 2(1):45–70.
15. Feldgun VR, Karinski YS, and Yankelevsky DZ (2013). A coupled approach to simulate the explosion response of a buried structure in a soil-rock layered medium. Int J Prot Struct 4(3):231–292.
16. Feldgun VR, Kochetkov AV, Karinski YS, and Yankelevsky DZ (2008a). Internal blast loading in a buried lined tunnel. Int J Impact Eng 35(3):172–183.
17. Feldgun VR, Kochetkov AV, Karinski YS, and Yankelevsky DZ (2008b). Blast response of a lined cavity in a porous saturated soil. Int J Impact Eng 35(9):953–966.
18. Felice, C. W., Gaffney, S., and Brown, J. A. (1991). Extended split-Hopkinson bar analysis for attenuating materials. *Journal of engineering mechanics*, *117*(5), 1119-1135.
19. Frye, J., and Lipner, N. (1983). *Determination of Soil Properties through Ground Motion Analysis*. Ballistic Missile Office, Norton AFB, CA.
20. Ghassemi A, Pak A, and Shahir H (2010). Numerical study of the coupled hydro–mechanical effects in dynamic compaction of saturated granular soils. Comput Geotech 37:10–24.
21. Goh, S. H., Lee, F. H., and Tan, T. S. (1998). Effects of lateral constraints and inertia on stress wave propagation in dry soil columns. *Geotechnique*, *48*(4), 449-463.
22. Grujicic M, Pandurangan B, and Cheeseman BA (2006). The effect of degree of saturation of sand on detonation phenomena associated with shallow-buried and ground-laid mines. Shock Vib 13:41–61.
23. Grujicic M, Pandurangan B, Cheeseman BA, Roy WN, Skaggs RR, Gupta R (2008a) Parameterization of the porous–material model for sand with various degrees of water saturation. Soil Dyn Earthq Eng 28:20–35
24. Grujicic M, Pandurangan B, Coutris N, Cheeseman BA, Roy WN, and Skaggs RR (2008b). Computer-simulations based development of a high strain–rate, large–deformation, highpressure material model for STANAG 4569 sandy gravel. Soil Dyn Earthq Eng 28:1045– 1062.
25. Hadala, P.F. (1973). Effect of Constitutive Properties of Earth Media on Outrunning Ground Shock from Large Explosions, Technical Report S-73-6 U.S. Army Engineer Waterways Experiment Station, Vicksburg, MS.
26. Hampton, D., and Wetzel, R. A. (1966). Stress wave propagation in confined soils. IIT Research Inst. Chicago IL.
27. Hendron Jr, A. J. (1963). The Behavior of Sand in One-Dimensional Compression. Ph. D. Thesis, Department of Civil Engineering, University of Illinois, Urbana.
28. Hendron Jr, A. J., Davisson, M. T., and Parola, J. F. (1969). Effect of Degree of Saturation on Compressibility of Soils from the Defence Research Establishment, Suffield (No. AEWESCR-S-69-3). Army engineer waterways experiment station Vicksburg MS.
29. Hendron, A.J., and Davisson, M.T. (1964). Static and Dynamic Constrained Moduli of Frenchman Flat Soils, Proceedings of the Symposium on Soil Structure Interaction. Tucson: The University of Arizona.

30. Henrych J (1979). The dynamics of explosion and its use. Elsevier, New York
31. Higgins, W., Chakraborty, T., and Basu, D. (2013). A high strain‐rate constitutive model for sand and its application in finite‐element analysis of tunnels subjected to blast. International Journal for Numerical and Analytical Methods in Geomechanics, 37(15), 2590-2610.
32. Higgins, William T. IV (2011). Development of a High Strain-Rate Constitutive Model for Sands and its Application in Finite Element Analysis of Tunnels Subjected to Blast. Master's Theses. University of Connecticut.
33. Isenberg, J. (1972). Nuclear Geoplosics-A Sourcebook of Underground Phenomena and Effects of Nuclear Explosions. Part 2. Mechanical Properties of Earth Materials (No. AA-R7120-2000). Agbabian Associates El Segundo CA.
34. Jackson, J. G., Jr., Ehrgott, J. Q., and Rohani, B. (1980). Loading rate effects on the compressibility of sand. J. Geotech. Engrg. Div., ASCE, 108(8), 829-852.
35. Kabir, M. E., Song, B., Martin, B. E., and Chen, W. (2010). Compressive behavior of fine sand. Sandia National Laboratories, New Mexico.
36. Karinski YS, Feldgun VR, and Yankelevsky DZ (2009a). Explosion induced dynamic soil– structure interaction analysis with the coupled Godunov-variational difference approach. Int J Numer Methods Eng 77:824–851.
37. Karinski YS, Feldgun VR, and Yankelevsky DZ (2009b). Effect of soil locking on the cylindrical shock wave's peak pressure attenuation. J Eng Mech ASCE 135(10):1166–1180.
38. Kondner, R. L. (1963). Hyperbolic stress-strain response: cohesive soils. J. Geotech. Engrg. Div., 89(1), 115-143.
39. Kramer, S.L. (1996). Geotechnical Earthquake Engineering, Prentice-Hall civil engineering and engineering mechanics series, Upper Saddle River, New Jersey. ISBN 0-13-374943-6.
40. Lewis BA (2004). Manual for LS–DYNA soil material model 147. Federal highway administration. Publication No. FHWA–HRT–095, McLean.
41. Lu G and Fall M (2017). Modelling blast wave propagation in a subsurface geotechnical structure made of an evolutive porous material. Mech Mater 108:21–39.
42. Lu, G. and Fall, M. (2018). State-of-the-art modelling of soil behaviour under blast loading. Geotechnical and Geological Engineering, 1-25.
43. Lumb, P. (1974). Application of statistics in soil mechanics, 'Soil Mechanics - new horizons', pp.44-111, Newness Butterworths, London.
44. Lyakhov GM (1974). Fundamentals of the dynamics of detonation waves in soils and rock. Nedra, Moscow.
45. Martin, B. E., Chen, W., Song, B., and Akers, S. A. (2009). Moisture effects on the high strain-rate behavior of sand. Mechanics of Materials, 41(6), 786-798.
46. McCormick, J.M., Baron, M.L., and Nelson, I. (1968). Studies on the Distant Plain 1A Event, DASA 2213. New York: Paul Weidlinger Consulting Engineers, 7/68. (AD 849944L)
47. Mei, G. X., Chen, R., and Liu, J. (2017). New Insight into Developing Mathematical Models for Predicting Deformation-Dependent Lateral Earth Pressure. International Journal of Geomechanics, 06017003.
48. Mellah, R., Auvinet, G., and Masrouri, F. (2000). Stochastic finite element method applied to non-linear analysis of embankments. Probabilistic Engineering Mechanics, 15(3), 251-259.
49. Nowatzki, E. A. (1965). A non-linear analysis of the surface ground displacement due to a nuclear air burst. Master of Science Thesis. The University of Arizona, USA.

50. Omidvar, M., Iskander, M., and Bless, S. (2012). Stress-strain behavior of sand at high strain rates. International journal of impact engineering, 49, 192-213.
51. Pathak, S., and Ramana, G. V. (2018). A Stress-Strain Model for Geomaterials Subjected to Air-Blast. In GeoShanghai International Conference (pp. 388-396). Springer, Singapore.
52. Pellegrino, A., De Cola, F., Dragnevski, K., and Petrinic, N. (2016). The Dynamic Response of Etnean Sand and the Effect of its Impingement on Ti-6Al-4 V Alloy. J. dynamic behavior mater. (2) 438–451.
53. Phoon, K.K., and Kulhawy, F.H. (1999a). Characterization of geotechnical variability. Canadian Geotechnical Journal, 36(4): 612–624.
54. Phoon, K.K. and Kulhawy, F.H. (1999b). Evaluation of geotechnical property variability, Canadian Geotechnical J., 36: 625-639.
55. Prapaharan S, Chameau JL, and Holtz RD (1989). Effect of strain rate on undrained strength derived from pressuremeter tests. Geotechnique 39(4):615–624.
56. Puzrin, A. M., and Burland, J. B. (1996). A logarithmic stress-strain function for rocks and soils. Geotechnique, 46(1), 157-164.
57. Ramberg, W., and Osgood, W.R. (1943). Description of Stress-Strain Curves by Three Parameters. NACA, TN902.
58. Roberts JE and de Souza JM (1958). The compressibility of sands. ASTM Proceedings No. 58.
59. Rohani, B. (1999). Theoretical Studies of Stress Wave Propagation in Laterally Confined Soils (No. WES/MP/SL-99-1). Army Engineer Waterways Experiment Station Vicksburg MS Structures Lab.
60. Salvadori, M., R. Skalak and P. Weidlinger (1960). Waves and Shocks in Locking and Dissipative Media, Proceedings ASCE, Vol. 86, No. EW2.
61. Schindler, L. (1968). Design and evaluation of a device for determining the one dimensional compression characteristics of soils subjected to impulse-type loads, PhD thesis, University of Illinois, in Urbana, Illinois.
62. Semblat, J., Luong, M. P., and Gary, G. (1999). 3D-Hopkinson bar: new experiments for dynamic testing on soils. Soils and foundations, 39(1), 1-10.
63. Simo JC, Kennedy JG, and Govindjee S (1988). Non-smooth multisurface plasticity and viscoplasticity. Loading/unloading conditions and numerical algorithms. Int J Numer Methods Eng 26:2161–2185
64. Skalak, R. and Weidlinger, P. (1961) Attenuation of stress waves in bi-linear materials. Journal of the Engineering Mechanics Division, 87(3), p. 1-12.
65. Smith, R. H. and Newmark, N. M. (1958). Numerical Integration for One-Dimensional Stress Waves, Civil Engineering Studies, Structural Research Series No. 162, University of Illinois, Urbana, Illinois.
66. Song, B., Chen, W., and Luk, V. (2009). Impact compressive response of dry sand. Mechanics of Materials, 41(6), 777-785.
67. Tong, X., and Tuan, C. Y. (2007). Viscoplastic cap model for soils under high strain rate loading. Journal of Geotechnical and Geoenvironmental Engineering, 133(2), 206-214.
68. Vanmarcke, E.H. (1977). Probabilistic modeling of soil profiles, Journal of the. Geotechnical Engineering Division, ASCE, Vol.103, No.GT11, pp.1227-1246.
69. Veyera, G. E. (1994). Uniaxial stress-strain behavior of unsaturated soils at high strain rates (No. WL-TR-93-3523). Wright Lab Tyndall AFB FL.
70. Wang Z, Lu Y, and Bai C (2008). Numerical analysis of blast-induced liquefaction of soil. Comput Geotech 5:196–209.

71. Wang Z, Lu Y, and Bai C (2011). Numerical simulation of explosion induced soil liquefaction and its effect on surface structures. Finite Elem Anal Des 47(9):1079–1090.
72. Wang Z, Lu Y, and Hao H (2004b). Numerical investigation of effects of water saturation on blast wave propagation in soil mass. J Eng Mech ASCE 130(5):551–561.
73. Wang, S., Shen, L., Maggi, F., El-Zein, A., and Nguyen, G. D. (2017). Uniaxial compressive behavior of partially saturated granular media under high strain rates. International Journal of Impact Engineering, 102, 156-168.
74. Wang, Z., and Lu, Y. (2003). Numerical analysis on dynamic deformation mechanism of soils under blast loading. Soil Dynamics and Earthquake Engineering, 23(8), 705-714.
75. Wang, Z., Hao, H., and Lu, Y. (2004a). A three-phase soil model for simulating stress wave propagation due to blast loading. International Journal for Numerical and Analytical Methods in Geomechanics, 28(1), 33-56.
76. Weidlinger, P. and Matthews, A. T. (1965). Shock and Reflection in a Nonlinear Medium, Proceedings, American Society of Civil Engineers, Paper No. 4375 (EM-3), 1.147.
77. Whitman, R. V. (1970). The Response of Soils to Dynamic Loadings; Report 26, Final Report. AD708625, US Army Engineer Waterways Experiment Station, Vicksburg.
78. Wilson, S. D., and Sibley, E. A. (1962). Ground Displacement From Air-Blast Loading, Journal of the Soil Mechanics and Foundations Division, ASCE 88 (SM6), 1-31.
79. Xia, K., Jafari, M., Kanopoulos, P. P., and Wei, Y. (2015). Constitutive Modelling of Soils under High Strain Rates: theoretical, numerical, and experimental results. Contract Report DRDC-RDDC-2015-C071, Department of Civil Engineering, University of Toronto, Toronto, Ontario
80. Xu TH, and Zhang LM. (2015). Numerical implementation of a bounding surface plasticity model for sand under high strain-rate loadings in LS–DYNA. Comput Geotech 66:203–218.
81. Yamamuro JA and Lade PV (1993). Effects of strain rate on instability of granular soils. Geotech Test J 16(3):304–313
82. Yamamuro JA, Bopp PA, and Lade PV (1996). One-dimensional compression of sands at high pressures. J. Geotech. Engrg., 122(2): 147-154.